Phase Separation in Lean-Grade Duplex Stainless Steel 2101

Citation	Garfinkel, D. A., Poplawsky, J. D., Guo, W., Young, G. A., & Tucker, J. D. (2015). Phase Separation in Lean-Grade Duplex Stainless Steel 2101. JOM Journal of the Minerals, Metals and Materials Society, 67(10), 2216-2222. doi:10.1007/s11837-015-1581-7
DOI	10.1007/s11837-015-1581-7
Publisher	Springer
Version	Version of Record
Terms of Use	http://cdss.library.oregonstate.edu/sa-termsofuse

JOM, Vol. 67, No. 10, 2015
DOI: 10.1007/s11837-015-1581-7

Phase Separation in Lean-Grade Duplex Stainless Steel 2101

DAVID A. GARFINKEL,[1] JONATHAN D. POPLAWSKY,[2] WEI GUO,[2] GEORGE A. YOUNG,[3] and JULIE D. TUCKER[1,4]

1.—School of Mechanical, Industrial and Manufacturing Engineering, Oregon State University, Corvallis, OR, USA. 2.—Center for Nanophase Materials Sciences, Oak Ridge National Laboratory, Oak Ridge, TN, USA. 3.—Knolls Atomic Power Laboratory, Schenectady, NY, USA. 4.—e-mail: julie.tucker@oregonstate.edu

The use of duplex stainless steels (DSS) in nuclear power generation systems is limited by thermal instability that leads to embrittlement in the temperature range of 204°C to 538°C. New lean-grade alloys, such as 2101, offer the potential to mitigate these effects. Thermal embrittlement was quantified through impact toughness and hardness testing on samples of alloy 2101 after aging at 427°C for various durations (1–10,000 h). Additionally, atom probe tomography (APT) was utilized in order to observe the kinetics of α–α' separation and G-phase formation. Mechanical testing and APT data for two other DSS alloys, 2003 and 2205, were used as a reference to 2101. The results show that alloy 2101 exhibits superior performance compared to the standard-grade DSS alloy 2205 but inferior to the lean-grade alloy 2003 in mechanical testing. APT data demonstrate that the degree of α–α' separation found in alloy 2101 closely resembles that of 2205 and greatly exceeds 2003. Additionally, contrary to what was observed in 2003, 2101 demonstrated G-phase like precipitates after long aging times, although precipitates were not as abundant as was observed in 2205.

INTRODUCTION

Duplex stainless steels (DSS) offer a desirable combination of strength, toughness, corrosion resistance, and affordability. These properties are the result of the duplex microstructure, which is composed of an approximately equal weight percentage of austenite and ferrite.[1] Due to this attractive combination of material properties, DSS are currently used in storage, chemical processing, desalinization, and other industries.[2] Additionally, DSS are a cost-effective alternative to Ni-based alloys currently used as piping in power generation systems.[3] However, thermal instabilities at high service temperatures limit use in these applications.

In the temperature range of 204°C to 538°C, a miscibility gap in the Fe-Cr system causes α–α' phase separation within the ferrite grains through either spinodal decomposition or nucleation and growth.[2] The resultant Cr-rich (α') and Cr-poor (α) regions produce a material with degraded mechanical properties. Although α–α' phase separation is limited to the ferrite grains, the loss of mechanical properties is observed in the overall material. The most notable changes are embrittlement and a reduction of corrosion resistance. In addition to α–α' phase separation, G-phase can also occur through nucleation and growth. Although it is clear that G-phase plays a role in the thermal embrittlement of DSS, the extent of its contribution is not conclusive. Experiments attempting to isolate G-phase precipitates from α–α' separation in order to observe the contribution of G-phase on embrittlement have yielded starkly different results.[4,5] It was concluded in Ref. 5 that G-phase precipitates had a minimal effect on mechanical testing, whereas Ref. 4 found that the presence of G-phase precipitates played a significant role in embrittlement.

The alloy composition has a significant impact on the thermal stability of DSS alloys.[6] In particular, increasing the amount of Cr-equivalent (Cr, Si, Mo, etc.) and Ni-equivalent (Ni, Mn, Cu, N, C, etc.) elements tends to shift thermal degradation to earlier times.[7] However, due to the complexity of alloying interactions, this trend might not always be observed.[1] A subset of DSS alloys, called lean-grade alloys, are manufactured with a reduction of Cr-equivalent and Ni-equivalent elements. Minimizing

(Published online August 19, 2015)

the use of Cr- and Ni-equivalent elements has the potential to delay phase transformation and thus to improve performance of DSS.[7] Equations 1 and 2 are used to determine the amount of Cr- and Ni-equivalent elements that are in an alloy.[8]

$$\mathrm{Cr_{eq}(wt.\%)} = \mathrm{Cr} + 2\mathrm{Si} + 1.5\mathrm{Mo} + 5\mathrm{V} + 5.5\mathrm{Al} + 1.75\mathrm{Nb} + 1.5\mathrm{Ti} + 0.75\mathrm{W} \quad (1)$$

$$\mathrm{Ni_{eq}(wt.\%)} = \mathrm{Ni} + \mathrm{Co} + 0.5\mathrm{Mn} + 0.3\mathrm{Cu} + 25\mathrm{N} + 30\mathrm{C} \quad (2)$$

In this study, a lean-grade DSS alloy 2101 was subjected to isothermal aging over various durations and temperatures. The alloy was assessed through mechanical testing (microhardness and impact toughness) and atom probe tomography (APT). The results are compared with previously analyzed alloys: a standard-grade DSS alloy, 2205; and a lean-grade alloy, 2003.[2]

EXPERIMENTAL DETAILS

Materials and Isothermal Aging

The samples of 2101 were obtained from 2.54-cm-thick plates that were hot rolled and solution annealed above 1038°C and water quenched. Bulk material composition of alloys 2101, 2003, and 2205 are displayed in Table I. The lean-grade alloys 2101 and 2003 have reduced concentrations of Cr, Ni, Mo, and Cu compared with the standard alloy 2205. Conversely, 2101 has a relatively high concentration of Mn and Si compared with the other alloys. Cr- and Ni-equivalent contents were calculated using Eqs. 1 and 2, and are included in Table I. The lean-grade alloys 2101 and 2003 have a lower Cr- and Ni-equivalent content than the standard alloy 2205. Additionally, there is a slight difference in the ferrite/austenite volume fraction. Alloy 2101 is composed of 42.8% ferrite, whereas 2003 and 2205 have ferrite contents of 35% to 40%.[9]

Samples of 2101 were aged isothermally in an air furnace at a temperature of 427°C and air cooled. Isothermal aging was conducted for durations of 1–10,000 h.

Impact Toughness

Charpy V-notch impact samples were machined from the aged plates in the traverse-short (T-S) orientation. Testing temperatures (–101°C to 204°C) and sample dimensions were in accordance with ASTM E23.[10] At least two samples were tested at each temperature to verify the accuracy of results.

Microhardness

Microhardness samples were polished and etched on the short-long (S-L) surface. Using a Vickers indenter and a load of 10 gf, measurements were taken in the ferrite grains. The small load is in compliance with ASTM standards to ensure edge effects from the boundary were avoided.[11] To limit variability in the data, no less than 10 measurements were taken for each aging time/temperature combination.

Atom Probe Tomography

Site-specific focused ion beam (FIB) liftouts were taken from the ferrite phase of the material, which could easily be identified after the alloy was mechanically polished and lightly etched.[12] Several sections of the liftout were mounted on microtip array posts that were each annularly milled (30 kV) and cleaned with a 5-kV ion beam to make needle-shaped specimens suitable for field evaporation. The resulting needle-shaped specimens were processed using a CAMECA Instruments LEAP 4000X HR local electrode atom probe (Cameca Instruments, Gennevilliers, France), which is equipped with an energy-compensating reflectron lens for improved mass resolution. The field evaporation of the specimens was performed with the following conditions: 200-kHz pulse repetition rate, 50 K specimen temperature, 20% pulse fraction, and a 0.3% to 0.5% detection rate. The resulting data were reconstructed and analyzed using the CAMECA IVAS software. Gallium enrichment from the FIB-based specimen preparation method was not an issue because of the well-cleaned needles.

RESULTS

Impact Toughness

The α–α' phase transformation that occurs with thermal aging causes a reduction in impact toughness. Figure 1 shows impact toughness as a function of testing temperature for alloys 2101, 2205, and 2003 aged at 427°C for 1000 h. The lean-grade alloys (2101 and 2003) both exhibit a more desirable performance than that of the standard alloy (2205); however, 2003 significantly outperforms 2101.

Table I. Duplex stainless steel alloy compositions (wt.%)

Alloy	Heat	Fe	Cr	Ni	Mo	Mn	Si	N	C	S	P	Cu	Al	Co	$\mathrm{Cr_{eq}}$	$\mathrm{Ni_{eq}}$
2101	844,962	Bal.	21.49	0.21	0.21	5.00	0.79	0.21	0.029	0.001	0.024	0.30	0.02	0.05	23.5	8.97
2003[3]	511,794	Bal.	21.42	3.70	1.75	1.22	0.37	0.180	0.010	0.0008	0.024	0.13	0.01	NR	24.8	9.15
2205[3]	827,616	Bal.	22.44	5.69	3.11	1.80	0.42	0.17	0.020	0.0004	0.028	0.43	NR	0.33	27.9	11.9

NR not reported.

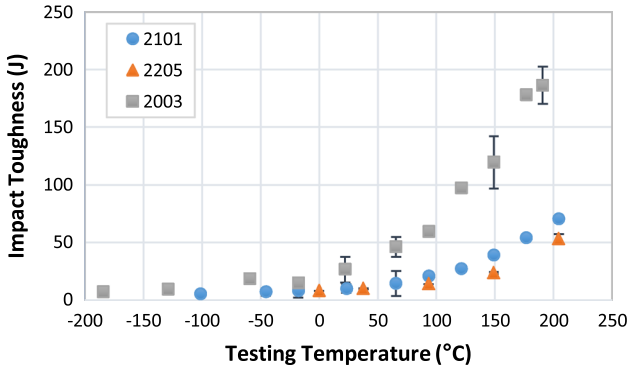

Fig. 1. Impact toughness versus testing temperature for alloys 2101, 2205,[3] and 2003[3] after aging at 427°C for 1000 h.

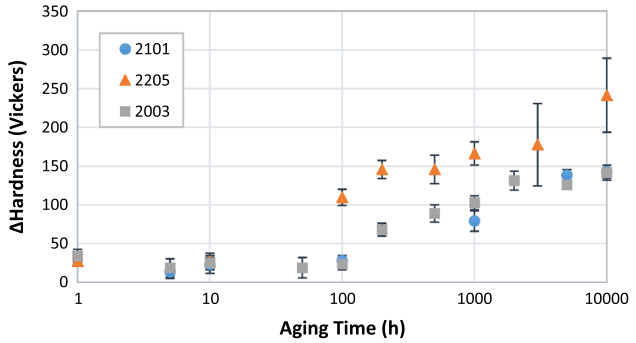

Fig. 2. Microhardness of alloys 2101, 2003,[3] and 2205[3] in the ferrite grains as a function of aging time at 427°C.

Furthermore, the lean-grade alloy 2101 exhibits a performance much closer to that of the standard alloy than the other lean alloy. Because of the relatively low concentration of Cr- and Ni-equivalent elements in 2101, a performance similar to or superior than 2003 would be expected; however, the results from impact toughness testing contradict this hypothesis. This behavior can be explained partly due to the greater amount of ferrite present in 2101 than 2003 and 2205. Because the phase transformation occurs exclusively in the ferrite grains, a material with a larger volume fraction of ferrite would be expected to have a more significant reduction in performance. However, the difference in the ferrite volume fraction is minimal and likely only plays a minor role in the relatively poor performance of 2101 in impact toughness testing.

Microhardness

In addition to a decrease in impact toughness, the hardness within the ferrite grains increases with thermal aging. Unlike impact toughness testing, the hardness within the ferrite grains can be tested separately from the austenite grains. Because of differences in unaged hardness between the alloys, the hardness values for each alloy were normalized with the initial hardness of that alloy. The initial hardness of 2101, 2205, and 2003 were 192, 237, and 227 respectively. The relationship between hardness and aging time for alloys 2101, 2205, and 2003 at an aging temperature of 427°C is shown in Fig. 2.

After short durations of aging (1–10 h), there is very little difference in the performance of the three alloys. After 100 h, however, alloy 2205 demonstrates significantly more hardening than the lean-grade alloys. The two lean-grade alloys exhibit a very similar response to aging; alloy 2101 demonstrated a slightly larger change in hardness than 2003 after long aging times. Although the changes in hardness exhibited by 2101 and 2003 are very similar, the lower unaged hardness of 2101 results in a percentage increase in hardness that is more than 10% larger in 2101 than 2003 for aging times of 5000 and 10,000 h.

Atom Probe Tomography

α–α' *Separation*

APT was conducted on four samples of alloy 2101. The samples were aged at 427°C for durations of 1, 100, 1000 and 10,000 h. Figure 3 displays the distribution of Cr, Mn, and Si atoms for each of the four aging times in a $40 \times 15 \times 5$ nm^3 volume of the APT sample. The cross section shows the dimensions of 40 nm width and 15 nm height, whereas the final dimension represents the depth into the page.

Cr distribution transitions from an essentially homogeneous distribution following 1 h of aging into distinct Cr-rich (blue) and Cr-depleted (white) regions after 100 h of aging. The presence of Cr-rich and Cr-depleted regions signifies the onset of α–α' separation. With continued aging, the Cr-rich regions increase in both concentration and size. The 100- and 1000-h samples exhibit an interconnected sinusoidal concentration gradient signifying spinodal decomposition. Note that the interconnected Cr-rich regions are more easily observed in the full three-dimensional reconstruction of the data (not shown) than in Fig. 3; however, smaller viewing volumes provide easier comparison between samples. After 10,000 h of aging, the Cr-rich regions have become so large that it is difficult to discern the degree of interconnectedness. Thus, it is difficult to be certain that the method of phase transformation remains spinodal decomposition.

In addition to the contribution of Cr to the α–α' separation, Mn and Si demonstrate a similar behavior. As was the case with Cr, both Mn and Si demonstrate small enriched and depleted regions that grow with increased aging time. Furthermore, Mn- and Si-enriched regions occur in the same regions as Cr enrichment. These regions are more difficult to see in Mn and Si due to a smaller degree of segregation. The contribution of Mn and Si to the α–α' separation is unexpected and was not observed in alloys 2003 and 2205.[3] This can be attributed, at least in part, to the much higher concentrations of Mn and Si in 2101 compared with alloys 2205 or 2003.

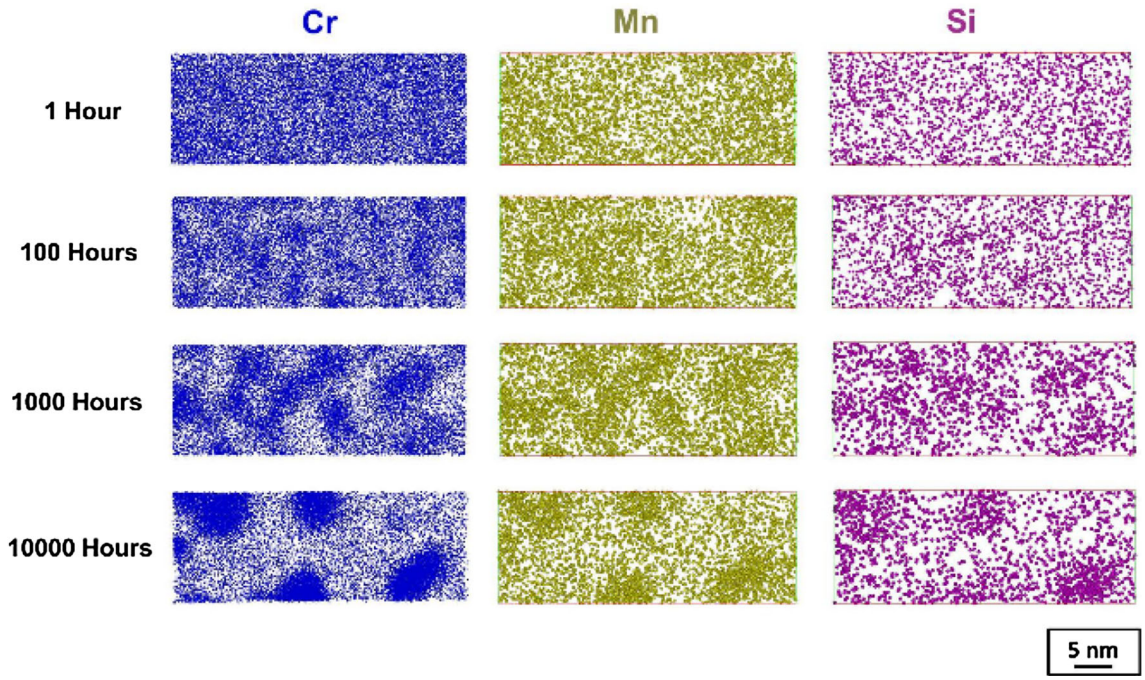

Fig. 3. Alloy 2101 α–α′ separation in Cr, Mn, and Si shown in 40 nm × 15 nm × 5 nm sections as a function of aging time.

To quantify α–α′ separation, the Langer-Bar-on-Miller (LBM) nonlinear theory of spinodal decomposition was used.[13] The LBM method fits two peaks into a frequency distribution of Cr concentrations to determine the average Cr concentration in the Cr-rich and Cr-depleted regions. The difference of these two peaks gives a value ΔCr, which represents the degree of α–α′ separation. Values of ΔCr for 2101, 2205, and 2003 as a function of aging time are shown in Fig. 4. To ensure consistency with LBM results for 2101, the values displayed in Fig. 4 demonstrate the ΔCr values of 2003 and 2205 after Ga-damaged regions were removed. This results in a slight increase in ΔCr values compared with Ref. 3. Alloy 2101 exhibits a low value of ΔCr after 1 h of aging, and it experiences large increases in ΔCr with each subsequent aging. This observation is in agreement with the trends observed in Fig. 3: minimal phase separation after short aging transitioning into large phase separation after longer aging times.

Figure 4 demonstrates that the relationship between ΔCr and aging time in 2101 and 2205 are essentially the same. Conversely, 2003 demonstrates less α–α′ separation than the other two alloys at all aging times except for 1 h. Thus, in terms of α–α′ separation, 2101 is exhibiting a behavior much closer to that of the standard alloy than the other lean alloy.

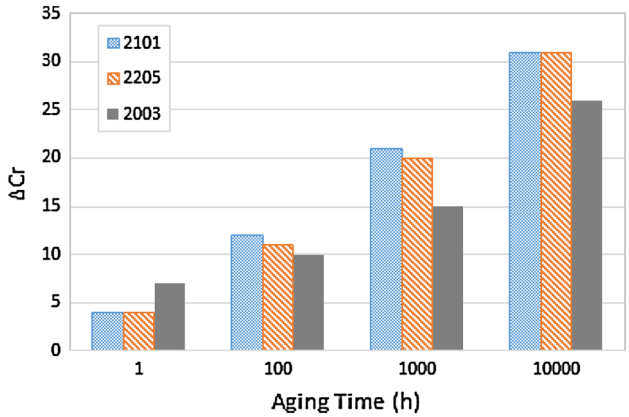

Fig. 4. ΔCr as a function of aging temperature for alloys 2101, 2205,[3] and 2003[3] using the LBM method.

Precipitate Formation

In addition to observing the relationship between thermal aging and α–α′ separation, APT also provided insights regarding precipitate formation, specifically G-phase. It is important to note that transmission electron microscopy was not conducted on 2101, so precipitates cannot be definitively identified as G-phase. However, the presence of Ni-rich clusters is a good indication of G-phase formation.[4]

Ni, Cu, and Mn distributions following 10,000 h of aging are displayed in Fig. 5. Because Ni, Cu, and Mn are less abundant in 2101 than Cr, the entire APT sample can be used to compare elemental distributions. Large Ni precipitates are observed sporadically throughout the sample. A comparison with Cr distributions revealed that these precipitates were located at the α–α′ interface. However, Cr reconstructions for the entire APT sample were not included in Fig. 5 due to the high concentration of particles, so this relationship is not seen in Fig. 5. Cu demonstrates a very similar distribution to Ni: Large

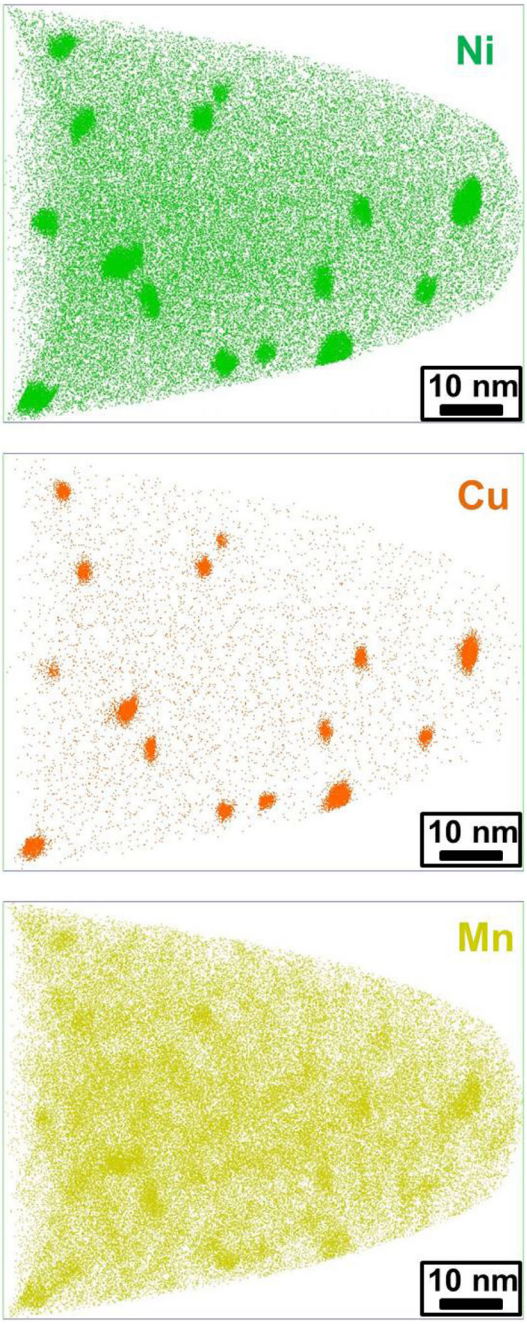

Fig. 5. APT analysis of Ni, Cu and Mn elemental distributions in alloy 2101 after 10,000 h of aging.

precipitates form in a nonconnected manner. Furthermore, the Cu precipitates are smaller than the Ni precipitates and appear to be oriented in the center of the Ni precipitates, such that there is a Cu-Ni nucleus-shell structure. Also in Fig. 5, it is shown that Mn contributes not only to α–α' separation but also to the Ni precipitates. The lack of an interconnected structure in the Ni, Cu, and Mn precipitates signifies a nucleation and growth process as opposed to spinodal decomposition. Additionally, the presence of precipitates at the α–α' interface provides further evidence that the precipitates are a form of G-phase.

The APT data for alloy 2003 did not show any precipitates, whereas 2205 demonstrated similar Ni precipitates as are seen in 2101. However, the Cu-Ni nucleus-shell structure was not observed in alloy 2205. The density of precipitates in alloys 2101 and 2205 are compared in Table II for different aging times. Table II shows that precipitates are far more abundant in alloy 2205 than 2101 for all aging times.

DISCUSSION

Much of the thermal embrittlement that occurs in DSS in the temperature range of 204°C to 538°C can be attributed to α–α' separation.[1] Thus, the lesser degree of α–α' separation in alloy 2003 compared with alloys 2101 and 2205 provides a viable explanation for the superior mechanical testing exhibited by 2003. However, this does not explain the discrepancy in mechanical testing between alloys 2101 and 2205; the two alloys demonstrated an essentially equal degree of α–α' separation after all aging times. Additionally, the microhardness performances of alloys 2101 and 2003 were much closer than would be expected based on of the differences in degree of α–α' separation.

The two primary differences in nanostructure observed between the alloys were the presence of Mn and Si in the α' region of alloy 2101, and the abundance of G-phase-type precipitates. The presence of G-phase type precipitates in 2101 and 2205 likely enhanced embrittlement in these two alloys. Furthermore, the greater concentration of precipitates in 2205 might contribute to the inferior mechanical testing exhibited by 2205 compared to 2101. However, the extent of the contribution of

Table II. Precipitate density in alloys 2101 and 2205 as a function of aging Time

	Precipitate number, density per $(100\ nm)^3$		
Alloy	**100 h**	**1000 h**	**10,000 h**
2101	16.0	103.4	59.6
2205	1251.1	350.8	532.5

these precipitates on embrittlement is unclear.[4,5] The presence of Mn and Si in the α–α′ separation may influence the lattice mismatch between the α and α′ regions, which could result in either reduced or increased embrittlement of 2101 compared with the other two alloys. Further analysis is required to determine the effect of Mn and Si on the lattice mismatch. Unfortunately, these differences do not provide a conclusive explanation for the discrepancy in mechanical testing compared with the degree of α–α′ separation observed, and additional testing and analysis for validation are required.

Another interesting result is the large difference in phase transformation between 2003 and 2101 despite a very similar Cr- and Ni-equivalent content. The α–α′ separation is likely in part a result of the significantly higher Mn content in 2101 as Mn has been shown to greatly accelerate the kinetics of α–α′ separation.[14] Furthermore, the presence of G-phase type precipitates in 2101 may promote α–α′ separation due to G-phase type precipitates accepting elements that are being expelled from the α and α′ regions.[1] Additionally, the presence of a Cu-Ni nucleus-shell structure in 2101 may be a sign of the Cu-rich ε phase acting as the nucleus.[15] The presence of Cu-rich precipitates can provide a nucleation site for G-phase formation and thus promote growth.[14] Despite a much higher Ni content in 2003 than 2101, the high Cu content in alloy 2101 may be the difference in G-phase type precipitates forming in 2101 and not 2003.

CONCLUSION

Mechanical testing combined with APT demonstrates that the lean-grade DSS alloy 2101 exhibits a thermal stability between that of alloys 2003 and 2205. The performance of 2101 in impact toughness testing was inferior to that of the other lean-grade alloy 2003 but superior to that of the standard-grade alloy 2205. In hardness testing, alloy 2101 demonstrated a behavior that was very similar to 2003 and superior to that of 2205. APT data show that 2101 exhibits a very similar degree of α–α′ separation as the standard-grade alloy 2205; however, 2205 had a much higher concentration of G-phase type precipitates. Additionally, 2101 demonstrated Mn and Si segregation into the α′ regions. This behavior was not observed in 2205 or 2003.

Combining the results of APT and mechanical testing demonstrates that different microstructural features may influence hardness and impact toughness testing differently. The degree of α–α′ separation appears to correlate with the impact toughness testing. Alloys 2101 and 2205 demonstrated a very similar degree of α–α′ separation, which was much higher than 2003. This closely mirrors the impact toughness results; 2003 had a much higher impact toughness than 2101 and 2205. The results from hardness testing are more difficult to explain with the APT results; however, it seems that G-phase type precipitation may influence hardness testing more than impact toughness testing. Alloy 2205 has the greatest abundance of precipitates and experiences the largest change in hardness. However, the similar behavior between 2101 and 2003 in hardness testing is difficult to explain with G-phase precipitation or α–α′ separation, and thus the segregation of Mn and Si in the α′ region could influence hardness behavior.

Because the lean-grade alloy 2101 had the lowest amount Cr- and Ni-equivalent elements, mechanical testing and APT results indicate that the reduced concentrations of Cr- and Ni-equivalent elements present in lean-grade DSS do not ensure superior thermal stability. Instead, the effects of each individual Cr- and Ni-equivalent element should be considered for a better prediction of performance.

Although α–α′ separation in the temperature range of 204°C to 538°C is the primary source of thermal embrittlement in DSS, it is not the only contributing factor. Mechanical testing demonstrated that only considering the degree of α–α′ separation does not accurately predict embrittlement of DSS alloys. For this reason, considering mechanical testing in parallel with nanostructure analysis has proven to be a powerful method for developing a further understanding of the behavior of thermally aged alloys.

ACKNOWLEDGEMENTS

This research was supported by ORNL's Center for Nanophase Materials Sciences (CNMS), which is a DOE Office of Science User Facility.

REFERENCES

1. R. Gunn, *Duplex Stainless Steels: Microstructure, Properties and Applications* (New York: Elsevier, 1997), pp. 14–47.
2. H.D. Solomon and T.M. Devine, *Duplex Stainless Steels: A Tale of Two Phases* (Materials Park: American Society for Metals, 1982), pp. 693–756.
3. J.D. Tucker, M.K. Miller, and G.A. Young, *Acta Mater.* 87, 15 (2015).
4. I. Shuro, H.H. Kuo, T. Sasaki, K. Hono, Y. Todaka, and M. Umemoto, *Mater. Sci. Eng., A* 552, 194 (2012).
5. S.L. Li, H.L. Zhang, Y.L. Wang, S.X. Li, K. Zheng, F. Xue, and X.T. Wang, *Mater. Sci. Eng., A* 564, 85 (2013).
6. D.H. Kang and W.H. Lee, *Metall. Mater. Trans. A* 43, 4678 (2012).
7. J.D. Tucker, G.A. Young Jr, and D.R. Eno, *Solid State Phenom.* 172–174, 331 (2011).
8. S. Lee, C.-Y. Lee, and Y.-K. Lee, *J. Alloys Compd.* 628, 46 (2015).
9. G.A. Young, J.D Tucker, N. Lewis, E. Plesko, and P. Sander, *Proceedings of the 15th International Conference on Environmental Degradation of Materials in Nuclear Power Systems—Water Reactors*, Colorado Springs, CO (2011), pp. 2369–2380.
10. ASTM Standard E23, 12c, Standard Test Methods for Notched Bar Impact Testing of Metallic Materials, 2012.
11. ASTM Standard E384, 11e1, Standard Test Method for Knoop and Vickers Hardness of Materials, 2011.
12. K. Thompson, D. Lawrence, D. Larson, J. Olson, and T. Kelly, *Ultramicroscopy* 107, 131 (2007).
13. J. Zhou, J. Odqvist, N. Thuvander, and P. Hedstom, *Microsc. Microanal.* 19, 665 (2013).

14. P. Hedström, F. Huyan, J. Zhou, S. Wessman, M. Thuvander, and J. Odqvist, *Mater. Sci. Eng., A* 574, 123 (2013).

15. J. Charles, *Duplex Stainless Steel—a Review after DSS '07 held in Grado*, presented at the Revue de Métallurgie, Grado, Italy (2008).